P5M.12 KATABATIC FLOW ALONG A DIFFERENTIALLY COOLED SLOPING SURFACE IN A STRATIFIED FLUID

Alan Shapiro* and Evgeni Fedorovich
School of Meteorology, University of Oklahoma, Norman, Oklahoma

1. INTRODUCTION

One of the remarkable successes of fluid dynamics in the last century was Prandtl's simple analytical model of katabatic and anabatic winds along mountains and valleys of constant slope. Prandtl's one-dimensional model was a solution of the Boussinesq equations of motion and thermodynamic energy for laminar flow of a viscous fluid along a uniformly cooled or heated sloping planar surface in a stably stratified fluid (1942). It had a boundary-layer character (a low-level jet topped by a weak reversed flow), and was exact within the Boussinesq framework: in the thermodynamic energy equation the along-slope advection of environmental (mean) temperature balanced thermal diffusion, while in the along-slope equation of motion the along-slope component of buoyancy balanced diffusion of the along-slope velocity component. With a suitable change of parameters, this same one-dimensional steady-state solution also described the along-slope flow and salinity (density) perturbations in an oceanic mixing layer at a sloping sidewall (Phillips 1970; Wunsch 1970). In this oceanic context, the flow was generated solenoidally by isopycnals that are forced to approach the sloping boundary at a right angle (zero normal flux). This same solution also described the free convective flow of a stratified fluid along heated vertical plates (Gill 1966, Elder 1965), and Ekman flow of a homogeneous viscous rotating fluid in the presence of an imposed wind stress or a stationary horizontal boundary (Pedlosky 1987). The equivalence of the Prandtl and Ekman models was a consequence of the analogy between stratified and rotating flows (Veronis 1970).

The Prandtl model has undergone several extensions and refinements within its one-dimensional framework. Gutman and Malbackov (1964), Lykosov and Gutman (1972), Gutman and Melgarejo (1981), and Gutman (1983) extended the model to include the Coriolis force, external winds, time dependence and simple but nonconstant eddy viscosities. Grisogono and Oerlemans (2001, 2002) considered more general vertical variations in the eddy viscosity and presented solutions valid in the WKB approximation. Observations (e.g., Oerlemans, 1998) suggest that despite its simplicity, when the model has appropriately tuned turbulence parameters, it provides a good description of slope flows at night and a reasonable approximation of the flows during the daytime. Observations indicate that the boundary layer depth in katabatic flows can be very small, ranging from a few hundred meters down to just a few meters. In the context of oceanic Ekman flows, Madsen (1977) described an extension of the classical framework to include a linearly-varying eddy viscosity and provision for unsteadiness (response to an impulsive surface wind stress). The imposition of nonconstant eddy viscosities resulted in more accurate velocity profiles.

In this study we extend the Prandtl framework to include surface buoyancy forcings that vary linearly with distance in the along-slope direction. This extended framework may apply in regions where buoyancy varies slowly enough in the along-slope direction that it is well-described locally by a linear variation. It may also apply to the case of a slowly-varying transition zone bridging two regions characterized by different constant katabatic forcings. In real applications, inhomogeneous surface forcings arise, for example, from differential snow/ice cover, differential cloud cover, differential shading (e.g., upper slopes are shaded while lower slopes are sunlit), differential soil moisture, and variations in land use.

The presence of a linearly-varying along-slope dependence to the surface buoyancy forcing breaks the symmetry of the classical Prandtl model and gives rise to flow acceleration, convergence and associated vertical motions, and horizontal and vertical advection of both perturbation and base-state temperature fields. Thus, the model is necessarily two-dimensional and nonlinear. However, as we will see, a simple scaling hypothesis (linear dependence of buoyancy and horizontal velocity components on the along-slope coordinate) removes the along-slope coordinate from the governing equations, and greatly simplifies the problem. With attention restricted to the steady-state flow structure, the Boussinesq equations of motion and thermodynamic energy reduce to a set of coupled nonlinear ordinary differential equations. Asymptotic solutions for the steady-state structure above the boundary layer are obtained. A key result is a formula for the inflow/outflow through the top of the boundary layer as a function of surface forcing (and environmental parameters that are used in the nondimensionalization). The asymptotic analyses are supplemented with nonlinear numerical integrations. Both the analytical and numerical analyses reveal an upper bound to surface buoyancy forcing (along-slope gradient) beyond which steady-state solutions do not exist.

* Corresponding author address: Alan Shapiro, School of Meteorology, University of Oklahoma, 100 East Boyd, Room 1310, Norman, Oklahoma, 73019; email: ashapiro@ou.edu

2. THE SIMILARITY MODEL AND ITS COROLLARIES

2.1 Boussinesq Equations for Two-dimensional Flow

We consider the following Boussinesq equations of thermodynamic energy, momentum, and mass conservation for nonhydrostatic buoyancy-driven flows of a stably-stratified fluid:

$$\frac{\partial B}{\partial T} + (\mathbf{V}\cdot\nabla)\,B = -N^2\,\mathbf{K^*}\cdot\mathbf{V} + \kappa_e\nabla^2 B\ , \qquad (2.1)$$

$$\frac{\partial \mathbf{V}}{\partial T} + (\mathbf{V}\cdot\nabla)\,\mathbf{V} = -\nabla\Pi + B\mathbf{K^*} + \nu_e\nabla^2\mathbf{V}\ , \qquad (2.2)$$

$$\nabla\cdot\mathbf{V} = 0\ . \qquad (2.3)$$

Here $\Pi \equiv (P - P_\infty)/\rho_r$ is the normalized perturbation pressure (P is pressure, P_∞ is environmental pressure, which is hydrostatic, ρ_r is a constant reference density), **V** is the two-dimensional velocity vector, T is time, and ν_e and κ_e are (constant) eddy viscosity and thermal diffusivity coefficients, respectively. **K*** is the unit vector associated with the Cartesian Z* axis, which points in the direction opposite the gravity vector **g**. $B \equiv |\mathbf{g}|\,(\theta - \theta_\infty)/\theta_r$ is the buoyancy force per unit mass, and $N \equiv \sqrt{(|\mathbf{g}|/\theta_r)\,d\theta_\infty/dZ^*}$ is the Brunt-Väisälä frequency (where θ is potential temperature, θ_∞ is a height-dependent environmental potential temperature, θ_r is a constant reference potential temperature). We consider θ_∞ to vary linearly with Z*, so N is constant. Although Coriolis terms are not included in our analysis, the model framework can be extended to include such terms. The neglect of the Coriolis terms is appropriate for flows with large Rossby numbers. For velocities typical of katabatic flows (say, 10 ms^{-1}) at mid- or upper-latitudes, our analysis should be appropriate for horizontal length scales on the order of 10 km or less.

The lower surface is an inclined planar boundary with slope angle α. We introduce a terrain-following Cartesian coordinate system (X, Y, Z) obtained from the original Cartesian system (X*, Y*, Z*) by a rotation through this slope angle (Fig. 1). The X-axis is the along (down) slope coordinate, and the Z-axis is the slope-normal coordinate. The Y and Y* axes coincide, and point in the cross-slope (into page) direction. The flow variables do not vary in the cross-slope direction. The unit vectors in the X*, Z* directions are **I***, **K***, respectively, while the corresponding unit vectors in the terrain-following coordinate system are **I**, **K**. Writing $\mathbf{V} = U\,\mathbf{I} + W\,\mathbf{K}$, and noting that **K*** only projects in the XZ plane (so $\mathbf{K^*}\cdot\mathbf{V} = U\,\mathbf{K^*}\cdot\mathbf{I} + W\,\mathbf{K^*}\cdot\mathbf{K} = -U\sin\alpha + W\cos\alpha$), (2.1)-(2.3) become

$$\frac{\partial B}{\partial T} + U\frac{\partial B}{\partial X} + W\frac{\partial B}{\partial Z} = U N^2\sin\alpha - W N^2\cos\alpha + \kappa_e\left(\frac{\partial^2 B}{\partial X^2} + \frac{\partial^2 B}{\partial Z^2}\right), \qquad (2.4)$$

$$\frac{\partial U}{\partial T} + U\frac{\partial U}{\partial X} + W\frac{\partial U}{\partial Z} = -\frac{\partial \Pi}{\partial X} - B\sin\alpha + \nu_e\left(\frac{\partial^2 U}{\partial X^2} + \frac{\partial^2 U}{\partial Z^2}\right), \qquad (2.5)$$

$$\frac{\partial W}{\partial T} + U\frac{\partial W}{\partial X} + W\frac{\partial W}{\partial Z} = -\frac{\partial \Pi}{\partial Z} + B\cos\alpha + \nu_e\left(\frac{\partial^2 W}{\partial X^2} + \frac{\partial^2 W}{\partial Z^2}\right), \qquad (2.6)$$

$$\frac{\partial U}{\partial X} + \frac{\partial W}{\partial Z} = 0\ . \qquad (2.7)$$

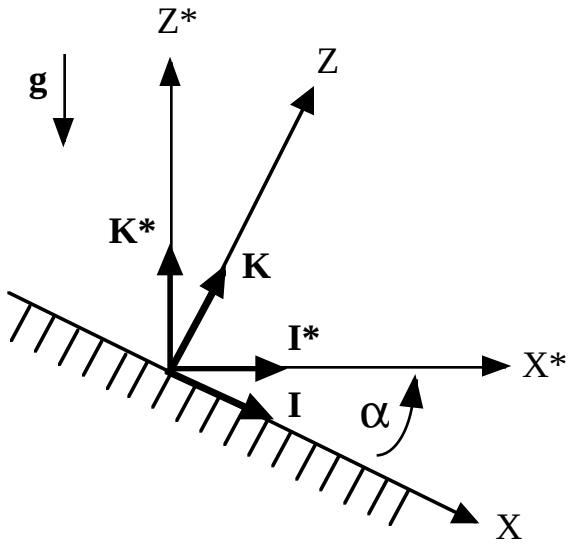

Fig. 1. Terrain-following coordinate system.

In terms of the nondimensional variables

$$x \equiv X\sqrt{\frac{N}{\nu_e}},\quad z \equiv Z\sqrt{\frac{N}{\nu_e}},\quad t \equiv N\,T,$$
$$b \equiv \frac{B}{N\sqrt{N\nu_e}},\quad u \equiv \frac{U}{\sqrt{N\nu_e}},\quad w \equiv \frac{W}{\sqrt{N\nu_e}},\quad \pi \equiv \frac{\Pi}{N\nu_e}, \qquad (2.8)$$

equations (2.4) - (2.7) become

$$\frac{\partial b}{\partial t} + u\frac{\partial b}{\partial x} + w\frac{\partial b}{\partial z} = u\sin\alpha - w\cos\alpha + \frac{1}{Pr}\left(\frac{\partial^2 b}{\partial x^2} + \frac{\partial^2 b}{\partial z^2}\right), \tag{2.9}$$

$$\frac{\partial u}{\partial t} + u\frac{\partial u}{\partial x} + w\frac{\partial u}{\partial z} = -\frac{\partial \pi}{\partial x} - b\sin\alpha + \frac{\partial^2 u}{\partial x^2} + \frac{\partial^2 u}{\partial z^2}, \tag{2.10}$$

$$\frac{\partial w}{\partial t} + u\frac{\partial w}{\partial x} + w\frac{\partial w}{\partial z} = -\frac{\partial \pi}{\partial z} + b\cos\alpha + \frac{\partial^2 w}{\partial x^2} + \frac{\partial^2 w}{\partial z^2}, \tag{2.11}$$

$$\frac{\partial u}{\partial x} + \frac{\partial w}{\partial z} = 0\ , \tag{2.12}$$

where $Pr \equiv \nu_e/\kappa_e$ is the Prandtl number.

Introducing the streamfunction ψ, defined by

$$u = \frac{\partial \psi}{\partial z}, \qquad w = -\frac{\partial \psi}{\partial x}\ , \tag{2.13}$$

equation (2.12) is automatically satisfied, while (2.9)-(2.11) become

$$\frac{\partial b}{\partial t} + \frac{\partial \psi}{\partial z}\frac{\partial b}{\partial x} - \frac{\partial \psi}{\partial x}\frac{\partial b}{\partial z} = \frac{\partial \psi}{\partial z}\sin\alpha + \frac{\partial \psi}{\partial x}\cos\alpha + \frac{1}{Pr}\left(\frac{\partial^2 b}{\partial x^2} + \frac{\partial^2 b}{\partial z^2}\right), \tag{2.14}$$

$$\frac{\partial^2 \psi}{\partial t\,\partial z} + \frac{\partial \psi}{\partial z}\frac{\partial^2 \psi}{\partial x\,\partial z} - \frac{\partial \psi}{\partial x}\frac{\partial^2 \psi}{\partial z^2} = -\frac{\partial \pi}{\partial x} - b\sin\alpha + \frac{\partial^3 \psi}{\partial x^2\,\partial z} + \frac{\partial^3 \psi}{\partial z^3}, \tag{2.15}$$

$$\frac{\partial^2 \psi}{\partial t\,\partial x} + \frac{\partial \psi}{\partial z}\frac{\partial^2 \psi}{\partial x^2} - \frac{\partial \psi}{\partial x}\frac{\partial^2 \psi}{\partial x\,\partial z} = \frac{\partial \pi}{\partial z} - b\cos\alpha + \frac{\partial^3 \psi}{\partial x^3} + \frac{\partial^3 \psi}{\partial z^2\,\partial x}. \tag{2.16}$$

2.2 The Similarity Model

We consider idealized flows driven by buoyancy fields that vary linearly in the along-slope (x) direction. Such distributions may provide good local approximations to actual buoyancy fields that vary sufficiently gradually with x. In view of (2.14), the corresponding streamfunction should also vary linearly with x, and so the along-slope velocity divergence $\partial u/\partial x$ and associated slope-normal velocity component w are independent of x. Equations (2.15) and (2.16) then indicate that the pressure can have up to a quadratic dependence on x, but the quadratic part must be independent of z. Such a quadratic term supports stagnation point flows but probably has little relevance for katabatic flows and will be omitted. Thus, the idealized flow is constrained to satisfy the similarity model,

$$\psi(x, z, t) = \psi_0(z, t) + x\,\psi_x(z, t), \tag{2.17}$$

$$b(x, z, t) = b_0(z, t) + x\,b_x(z, t), \tag{2.18}$$

$$\pi(x, z, t) = \pi_0(z, t) + x\,\pi_x(z, t). \tag{2.19}$$

Although our analysis proceeds in a streamfunction formulation, it may be useful to keep in mind that the velocity components consistent with this model are of the form $w = -\psi_x(z, t)$, and $u = u_0(z, t) + x\,u_x(z, t)$, where $u_0 = \partial\psi_0/\partial z$ and $u_x = \partial\psi_x/\partial z$. The functions ψ_0, ψ_x, u_0, u_x, w, b_0, b_x, π_0, π_x vary with z and t, but are independent of x. Substituting (2.17)-(2.19) into (2.14)-(2.16), and collecting terms in common powers of x, yields the partial differential equations,

$$\frac{\partial b_0}{\partial t} + \frac{\partial \psi_0}{\partial z}b_x - \psi_x\frac{\partial b_0}{\partial z} = \frac{\partial \psi_0}{\partial z}\sin\alpha + \psi_x\cos\alpha + \frac{1}{Pr}\frac{\partial^2 b_0}{\partial z^2}, \tag{2.20}$$

$$\frac{\partial b_x}{\partial t} + \frac{\partial \psi_x}{\partial z}b_x - \psi_x\frac{\partial b_x}{\partial z} = \frac{\partial \psi_x}{\partial z}\sin\alpha + \frac{1}{Pr}\frac{\partial^2 b_x}{\partial z^2}, \tag{2.21}$$

$$\frac{\partial^2 \psi_0}{\partial t\,\partial z} + \frac{\partial \psi_0}{\partial z}\frac{\partial \psi_x}{\partial z} - \psi_x\frac{\partial^2 \psi_0}{\partial z^2} = -\pi_x - b_0\sin\alpha + \frac{\partial^3 \psi_0}{\partial z^3}, \tag{2.22}$$

$$\frac{\partial^2 \psi_x}{\partial t\,\partial z} + \frac{\partial \psi_x}{\partial z}\frac{\partial \psi_x}{\partial z} - \psi_x\frac{\partial^2 \psi_x}{\partial z^2} = -b_x\sin\alpha + \frac{\partial^3 \psi_x}{\partial z^3}, \tag{2.23}$$

$$\frac{\partial \psi_x}{\partial t} - \psi_x\frac{\partial \psi_x}{\partial z} = \frac{\partial \pi_0}{\partial z} - b_0\cos\alpha + \frac{\partial^2 \psi_x}{\partial z^2}\ . \tag{2.24}$$

$$0 = \frac{\partial \pi_x}{\partial z} - b_x\cos\alpha\ . \tag{2.25}$$

Several features of (2.20)-(2.25) deserve mention. Firstly, in proceeding from (2.14)-(2.16) to (2.20)-(2.25), the number of independent variables has been reduced from three, (x, z, t), to two, (z, t). This greatly simplifies the problem. In particular, the steady state is described by ordinary differential equations rather than

partial differential equations. Secondly, the system (2.20)-(2.25) is exact within the Boussinesq framework, that is, for flows constrained to satisfy (2.17)-(2.19), the governing equations exactly reduce to (2.20)-(2.25). Analogous similarity models have led to exact solutions of the Navier-Stokes equations for planar stagnation-point flows (Schlichting 1979; Yang 1958), axisymmetric stagnation-point flows (Schlichting 1979; Williams 1968) and von Kármán-Bödewadt vortices (Zandbergen & Dijkstra 1987; Shapiro 2001), and to exact solutions of the nonlinear shallow-water equations for basins of elliptical cross-section and parabolic depth variation (Thacker 1981; Cushman-Roisin 1984, 1987; Cushman-Roisin et al. 1985; Shapiro 1996). Thirdly, there is a partial decoupling of the equations in (2.20)-(2.25), and this facilitates their solution. Equations (2.21) and (2.23) comprise a closed nonlinear system for ψ_x and b_x that can be solved first. The π_x variable can then be recovered from (2.25). Equations (2.20) and (2.22) then form a closed linear system for ψ_0, and b_0. Since ψ_0 always appears differentiated with respect to z, it will be convenient to solve for $\partial\psi_0/\partial z$ and b_0, and then obtain ψ_0 by integration. Finally, (2.24) can be integrated to obtain π_0. Since ψ_x, b_x, and π_x are associated with the divergent part of the velocity field, they will be refered to as divergent flow variables. Similarly, ψ_0, b_0, and π_0 will be referred to as nondivergent flow variables.

Since the $\partial^2/\partial x^2$ diffusion terms in (2.14)-(2.16) vanish identically within the framework of the similarity model, the suitability of the model in real applications hinges, in part, on when these diffusion terms can be safely neglected. A scale analysis shows that these terms are much smaller than the corresponding $\partial^2/\partial z^2$ diffusion terms and advection terms if $H/L << 1$ and $Re \equiv U_c L/\nu_e >> 1$. Here H and L are dimensional length scales in the slope-normal and along-slope directions, respectively, and U_c is a dimensional along-slope velocity scale. Thus, the model should be suitable for shallow (boundary-layer type) flows.

2.3 Divergent Flow Variables

Restricting attention to pure katabatic flows, (katabatic flows without an imposed pressure gradient, $\lim_{z\to\infty} \pi_x = 0$], three independent parameters appear in the divergent flow system: α, Pr and a surface buoyancy parameter (boundary condition). However, an equivalent system involving only two independent parameters, Pr and a scaled surface buoyancy parameter is obtained by the change of variables,

$$\eta \equiv \sqrt{\sin\alpha}\, z, \qquad \tau \equiv \sin\alpha\, t, \qquad f \equiv \sqrt{\csc\alpha}\, \psi_x, \qquad g \equiv \csc\alpha\, b_x. \tag{2.26}$$

In terms of these variables, (2.21) and (2.23) become

$$\frac{\partial g}{\partial \tau} + g\frac{\partial f}{\partial \eta} - f\frac{\partial g}{\partial \eta} = \frac{\partial f}{\partial \eta} + \frac{1}{\mathrm{Pr}}\frac{\partial^2 g}{\partial \eta^2}, \tag{2.27}$$

$$\frac{\partial^2 f}{\partial \tau\, \partial \eta} + \left(\frac{\partial f}{\partial \eta}\right)^2 - f\frac{\partial^2 f}{\partial \eta^2} = -g + \frac{\partial^3 f}{\partial \eta^3}, \tag{2.28}$$

equations in which α no longer appears. In the steady state, (2.27)-(2.28) reduce to the ordinary differential equations

$$g f' - f g' = f' + \frac{1}{\mathrm{Pr}} g'', \tag{2.29}$$

$$f'^2 - f f'' = -g + f''', \tag{2.30}$$

where a prime denotes differentiation with respect to η.

The boundary conditions are the remote conditions

$$\lim_{\eta\to\infty} f'(\eta) = \lim_{\eta\to\infty} g(\eta) = 0, \tag{2.31}$$

and the surface conditions

$$f(0) = 0, \quad \text{(impermeability)}, \tag{2.32}$$

$$f'(0) = 0, \quad \text{(no-slip on u-velocity component)}, \tag{2.33}$$

$$g(0) = \csc\alpha\, b_x(0), \quad \text{(along-slope gradient of b)}. \tag{2.34}$$

The only appearance of α in the divergent flow system is in boundary condition (2.34) where it is coupled with the along-slope buoyancy gradient.

Integrating (2.25) and applying the remote condition $\lim_{\eta\to\infty} \pi_x = 0$ yields

$$\pi_x = -\cos\alpha \sqrt{\sin\alpha} \int_\eta^\infty g(\bar\eta)\, d\bar\eta, \tag{2.35}$$

where an overbar denotes a dummy integration variable.

2.4 Nondivergent Flow Variables

For the nondivergent flow system we introduce the scaled variables,

$$k \equiv \sec\alpha \sqrt{\sin\alpha}\, \frac{\partial \psi_0}{\partial z}, \qquad h \equiv \sec\alpha \sqrt{\sin\alpha}\, b_0, \tag{2.36}$$

which reduce (2.20) and (2.22) [with (2.35) for π_x] to

$$\frac{\partial h}{\partial \tau} + g k - f\frac{\partial h}{\partial \eta} = k + f + \frac{1}{\mathrm{Pr}}\frac{\partial^2 h}{\partial \eta^2}, \tag{2.37}$$

$$\frac{\partial k}{\partial \tau} + k\frac{\partial f}{\partial \eta} - f\frac{\partial k}{\partial \eta} = \int_{\eta}^{\infty} g(\bar{\eta})\, d\bar{\eta} - h + \frac{\partial^2 k}{\partial \eta^2} \ . \quad (2.38)$$

Equations (2.37) and (2.38) are linear, but have inhomogeneous terms and variable coefficients.

In the steady state, (2.37) and (2.38) become the ordinary differential equations

$$g\,k - f\,h' = k + f + \frac{1}{Pr}\,h'' \ , \quad (2.39)$$

$$f'\,k - f\,k' = \int_{\eta}^{\infty} g(\bar{\eta})\, d\bar{\eta} - h + k'' \ . \quad (2.40)$$

This system is subject to the remote conditions

$$\lim_{\eta\to\infty} k'(\eta) = \lim_{\eta\to\infty} h(\eta) = 0 \ , \quad (2.41)$$

and the surface conditions

$$k(0) = 0, \quad \text{(no-slip on u-velocity component)}, \quad (2.42)$$

$$h(0) = \sec\alpha \sqrt{\sin\alpha}\, b_0(0) \ , \ \text{(surface buoyancy)}. \quad (2.43)$$

Again, α has been removed as an independent parameter from the differential equations. In this nondivergent flow system, α only appears in boundary condition (2.43) where it is coupled with the surface buoyancy.

According to (2.41), the slope-normal derivative of the u-velocity function (k' rather than k itself) vanishes at infinity. As will be discussed in the asymptotic analysis, the remote value of k insures that the remote flow is parallel to the isentropes.

Once (2.39)-(2.40) have been solved, we obtain ψ_0 from (2.36) and the impermeability condition as

$$\psi_0 = \cot\alpha \int_0^{\eta} k(\bar{\eta})\, d\bar{\eta} \ . \quad (2.44)$$

3. ASYMPTOTIC ANALYSIS OF THE STEADY STATE

An asymptotic analysis (valid for large η) of the divergent and nondivergent flow systems in pure katabatic flow is conducted for the steady state. Attention is restricted to a Prandtl number of unity.

The inhomogeneous surface buoyancy will, in the nonlinear system, induce an along-slope velocity divergence and associated subsidence (or ascent) through the depth of the boundary layer. The divergence vanishes at infinity, but its integral, the slope-normal velocity component, need not vanish:

$$\int_0^{\infty} \frac{\partial u}{\partial x}\, dz = \int_0^{\infty} \frac{d\psi_x}{dz}\, dz = \psi_x(\infty) = \frac{f(\infty)}{\sqrt{\csc\alpha}} \ .$$

This remote slope-normal velocity is analogous to the axial flow that occurs in von Kármán-Bödewadt vortices far above the plate boundary in response to centrifugal pumping near the boundary (Schlichting 1979). As we will see, it plays a key role in the asymptotic structure of both the divergent and nondivergent flow variables. As will be confirmed by the numerical integration of the full nonlinear system, the asymptotic analysis provides a good estimate of the remote slope-normal velocity component. It also yields an intriguing result, verified in the numerical integration, concerning the non-existence of steady state solutions for certain parameter values.

3.1 Asymptotic Analysis of the Divergent Flow Variables

With the remote slope-normal velocity component denoted by $a \equiv \lim_{\eta\to\infty} f(\eta)$, the perturbation slope-normal velocity component $\phi(\eta)$ is given by

$$\phi \equiv f - a \ . \quad (3.1)$$

The function g is assumed to vanish at infinity, along with ϕ. For η large enough, ϕ and g are sufficiently small that their products can be neglected, and (2.29) and (2.30) (with Pr = 1) linearize as

$$-\,a\,g' = \phi' + g'' \ , \quad (3.2)$$

$$-\,a\,\phi'' = -g + \phi''' \ . \quad (3.3)$$

Obtaining the solution of (3.2), (3.3) is straightforward but tedious. After much labor (steps omitted) one finds

$$g = A \exp\left[-\frac{\eta}{2}\left(a + |a|\sqrt{\gamma}\right)\right] \sin\left(\frac{|a|}{2}\sqrt{\gamma - 1}\ \eta + \varepsilon\right) \ , \quad (3.4)$$

$$\phi = -A\sqrt{\frac{a}{2}\left(a\gamma - |a|\sqrt{\gamma}\right)}\ \exp\left[-\frac{\eta}{2}\left(a + |a|\sqrt{\gamma}\right)\right] \times \sin\left(\frac{|a|}{2}\sqrt{\gamma - 1}\ \eta + \varepsilon + \delta\right), \quad (3.5)$$

where A and ε are as-yet undetermined constants, and γ and the phase-shift parameter δ are defined by

$$\gamma \equiv \frac{1}{2}\left(\sqrt{1 + \frac{16}{a^4}} + 1\right) > 1 \ , \quad (3.6)$$

$$\delta \equiv \tan^{-1}\left[-\frac{a}{2}\left(|a|\sqrt{\gamma} + a\gamma\right)\right], \quad \frac{\pi}{2} < \delta < \pi. \qquad (3.7)$$

Care should be taken in the evaluation of the inverse tangent in (3.7) to insure that δ appears in the second quadrant ($\pi/2 < \delta < \pi$). For large values of $|a|$, say, $|a| > 5$, (3.7) is well-approximated by $\delta \approx \pi/2$ for $a > 0$, and by $\delta \approx \pi$ for $a < 0$.

The asymptotic solutions for ϕ and g are in the form of a spatially-decaying oscillation. The wavelength λ and e-folding decay length scale L_e are $\lambda \equiv 4\pi/(|a|\sqrt{\gamma - 1})$, and $L_e \equiv 2/(a + |a|\sqrt{\gamma})$, respectively. For large values of $|a|$, λ is well-approximated by $\lambda \approx 2\pi|a|$, while L_e is well-approximated by $L_e \approx 1/a$ for $a > 0$, and $L_e \approx |a|^3$ for $a < 0$. For large positive values of a, L_e is very small, indicating rapid decay of g and ϕ. Figure 2 depicts λ and L_e for smaller values of $|a|$.

Although the asymptotic analysis is valid for large η, a surprisingly accurate formula for the remote slope-normal velocity component can be obtained by carrying the analysis down to the lower surface where the surface boundary conditions (2.32) - (2.34) can be imposed. It can be shown that the no-slip condition and imposed along-slope buoyancy gradient condition result in

$$\cos\varepsilon = 0, \quad A\sin\varepsilon = g(0). \qquad (3.8)$$

Imposing the impermeability condition (2.32) [in the form $\phi(0) = -a$] in (3.5) yields

$$a = A\sqrt{\frac{a}{2}\left(a\gamma - |a|\sqrt{\gamma}\right)}\,\sin(\varepsilon + \delta). \qquad (3.9)$$

In (3.9) we expand the $\sin(\varepsilon + \delta)$ term, and impose (3.8) and a formula for $\cos\delta$, [an intermediate result from the derivation of (3.7)] obtaining

$$a = \frac{g(0)}{2}\left(a - |a|\sqrt{\gamma}\right). \qquad (3.10)$$

Since $\gamma > 1$, (3.10) shows that a and g(0) have opposite signs. This is consistent with the intuitive notion that a surface buoyancy field that increases in the down-slope direction ($g > 0$) is associated with katabatic winds that weaken in the down-slope direction, convergence and rising motion ($w > 0$; $a < 0$). Using (3.6) for γ, (3.10) can readily be solved as

$$a = \pm 2\left\{\left[2\left(1 - \frac{2}{g(0)}\right)^2 - 1\right]^2 - 1\right\}^{-1/4} \qquad (3.11)$$

where we take the positive root if $g(0) < 0$, and the negative root if $g(0) > 0$. The remote slope-normal velocity component obtained from (3.11) and the corresponding values obtained from numerical integrations of the full nonlinear system are presented in Fig. 3.

Equation (3.11) also yields an intriguing result concerning the non-existence of solutions. If $g(0) > 1$, the quantity within curly brackets is negative, and its 1/4 root is complex. Hence a would be a complex quantity. However, this is physically impossible since a, which is a velocity component, must be real. This contradiction indicates a breakdown of the steady-state asymptotic solution for $g(0) > 1$.

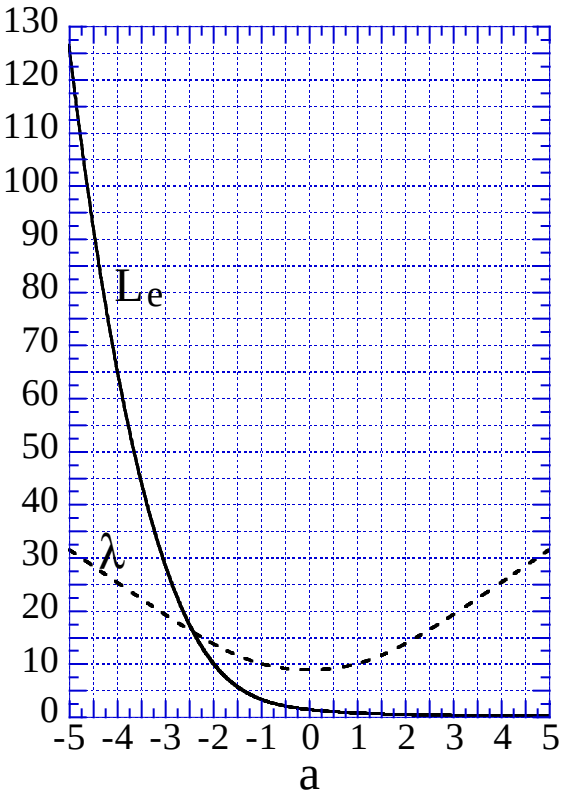

Fig. 2. Wavelength λ and length scale L_e as functions of the remote slope-normal velocity parameter a. All quantities are nondimensional.

3.2 Asymptotic Analysis of Nondivergent Flow Variables

In the limit $\eta \to \infty$, (2.39) yields $k + f \to 0$, or, since $f \to a$, $k \to -a$. These k and f terms originate in the thermodynamic energy equation (2.20), where they describe the along-slope and slope-normal advection of (environmental) potential temperature, respectively. As $\eta \to \infty$, these terms cancel. Thus, the remote flow is

parallel to the isentropes and there is no potential temperature advection.

Defining the perturbation along-slope velocity component $\kappa(\eta)$ by

$$\kappa \equiv k + a \,, \tag{3.12}$$

and noting that κ vanishes at infinity along with h, g and ϕ, (2.39) and (2.40) with Pr =1 can be approximated at large η as

$$-a\,g - a\,h' = \kappa + \phi + h'' \,, \tag{3.13}$$

$$-a\,\phi' - a\,\kappa' = \int_{\eta}^{\infty} g(\bar{\eta})\, d\bar{\eta} - h + \kappa'' \,. \tag{3.14}$$

After a lengthy derivation (steps omitted) the solution of (3.13) and (3.14) is obtained as

$$\kappa = \frac{A}{2}\frac{|a|}{a}\sqrt{\frac{2\sqrt{\gamma}}{2\gamma-1}\left(\sqrt{\gamma}+\frac{a}{|a|}\right)} \;\times$$
$$\eta\,\exp\left[-\left(a+|a|\sqrt{\gamma}\right)\frac{\eta}{2}\right]\cos\left(\frac{|a|}{2}\sqrt{\gamma-1}\;\eta+\varepsilon+\mu\right)$$
$$+\,E\exp\left[-\left(a+|a|\sqrt{\gamma}\right)\frac{\eta}{2}\right]\cos\left(\frac{|a|}{2}\sqrt{\gamma-1}\;\eta+\Lambda\right), \tag{3.15}$$

$$h = \frac{A}{2}\frac{|a|}{a}\sqrt{\frac{2\sqrt{\gamma}}{2\gamma-1}\left(\sqrt{\gamma}+\frac{a}{|a|}\right)} \;\times$$
$$\eta\,\exp\left[-\frac{\eta}{2}\left(a+|a|\sqrt{\gamma}\right)\right]\sin\left(\frac{|a|}{2}\sqrt{\gamma-1}\;\eta+\varepsilon+\mu\right)$$
$$+\,E\exp\left[-\frac{\eta}{2}\left(a+|a|\sqrt{\gamma}\right)\right]\sin\left(\frac{|a|}{2}\sqrt{\gamma-1}\;\eta+\Lambda\right), \tag{3.16}$$

where Λ is a phase shift (yet to be determined), and

$$\mu \equiv \tan^{-1}\left[\frac{|a|\sqrt{\gamma-1}}{a(2\gamma-1)+|a|\sqrt{\gamma}}\right]. \tag{3.17}$$

When evaluating the inverse tangent in (3.17), care should be taken to insure that if $a > 0$ then μ appears in the first quadrant ($0 < \mu < \pi/2$), but if $a < 0$ then μ appears in the second quadrant ($\pi/2 < \mu < \pi$).

As in the solutions for the divergent flow variables g and ϕ, the solutions for κ and h are comprised of oscillations of wavelength $\lambda \equiv 4\pi/(|a|\sqrt{\gamma-1})$. Since the envelope of the waves associated with the first terms in (3.15), (3.16) is $Q_{env} \equiv \eta\exp[-(a+|a|\sqrt{\gamma})\,\eta/2]$, these waves amplify prior to decaying. In contrast, the envelope of the g and ϕ waves provides only exponential decay. Setting the first and second derivatives of Q_{env} to zero yields the locations of the envelope maximum and inflection point as $2/(a+|a|\sqrt{\gamma})$ and $4/(a+|a|\sqrt{\gamma})$, respectively. It can readily be shown that an envelope width L_w defined as twice the distance between these maximum and inflection points is identical to the e-folding length scale in the divergent-flow solutions, that is, $L_w = L_e = 2/(a+|a|\sqrt{\gamma})$.

4. NUMERICAL ANALYSIS FOR Pr = 1

The structure of the divergent flow in the steady state for Pr = 1 is sought as the terminal state of the initial value problem consisting of the unsteady equations (2.27) and (2.28), boundary conditions (2.31)-(2.34) (imposed for $\tau > 0$), and an initial condition of no motion and no thermal perturbation of the boundary. The sudden imposition of a nonzero surface value of g and its maintenance for $\tau > 0$ [boundary condition (2.34)] drive the flow.

The initial value problem is solved with a variant of the Forward Time Centered Space (FTCS) finite difference algorithm (Fletcher 1988). Rather than work directly with f, we introduce a new variable $F \equiv \partial f/\partial\eta$, in terms of which f becomes $f = \int_0^{\eta} F(\bar{\eta})\, d\bar{\eta}$. The FTCS discretization of (2.27), (2.28) on a uniform grid in η-τ space [with trapezoidal rule for the discretization of $\int_0^{\eta} F(\bar{\eta})\, d\bar{\eta}$] yields the update formulas

$$g_m^{n+1} = g_m^n + \Delta\tau\left(1 - g_m^n\right)F_m^n + 0.5\,\Delta\tau\, I_m^n\left(g_{m+1}^n - g_{m-1}^n\right) + s\left(g_{m+1}^n - 2g_m^n + g_{m-1}^n\right), \tag{5.1}$$

$$F_m^{n+1} = F_m^n - \Delta\tau\,(F_m^n)^2 - \Delta\tau\, g_m^n + 0.5\,\Delta\tau\, I_m^n\left(F_{m+1}^n - F_{m-1}^n\right) + s\left(F_{m+1}^n - 2F_m^n + F_{m-1}^n\right), \tag{5.2}$$

where

$$I_m^n = I_{m-1}^n + 0.5\left(F_{m-1}^n + F_m^n\right); \quad m \geq 2,$$
$$= 0; \quad m = 1 \,, \tag{5.3}$$

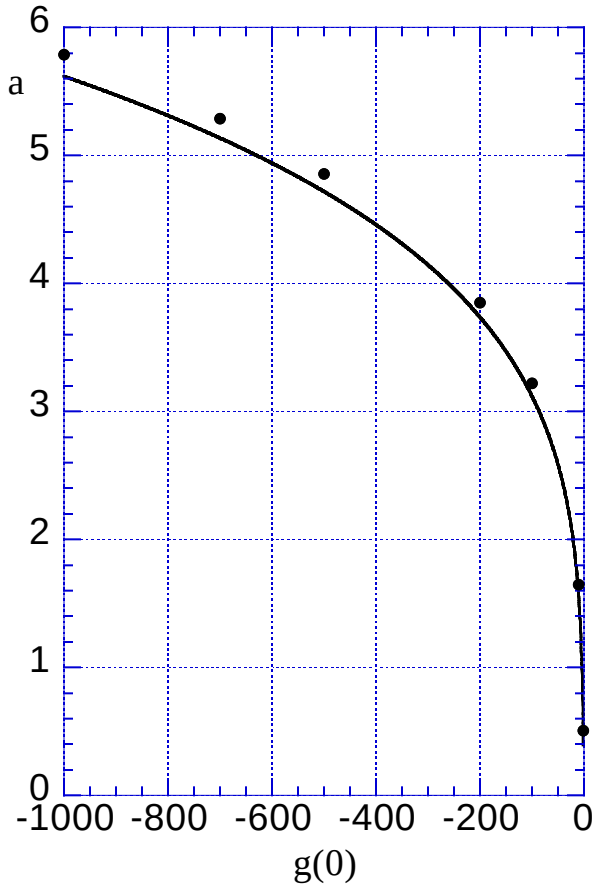

Fig. 3. Remote slope-normal velocity component as a function of the along-slope buoyancy gradient at the surface, g(0), in the steady state. Solid curve is the analytical solution (3.11) from the asymptotic analysis. Circles are values from the numerical solution after the transients had died out. Results are presented for negative values of g(0).

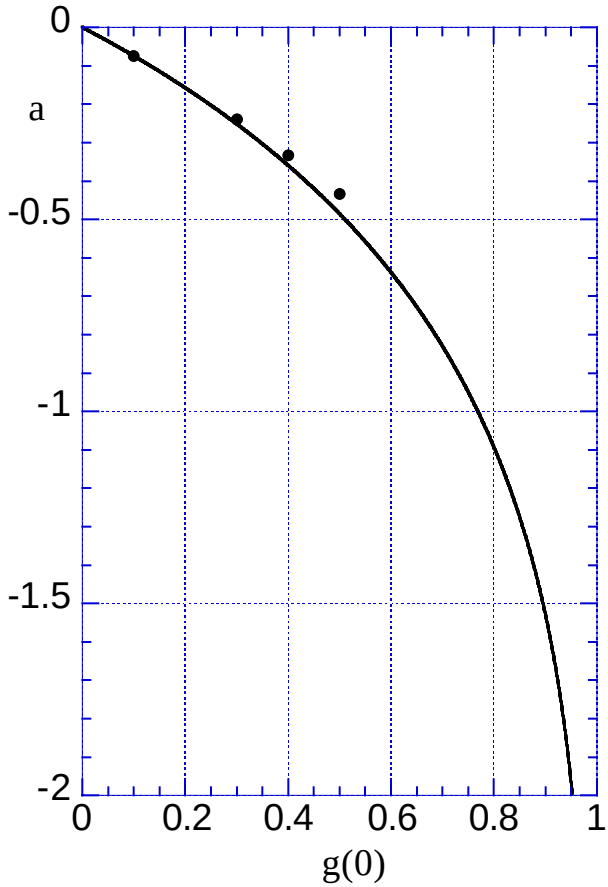

Fig. 4. As in Fig. 3 but for positive values of g(0). The value g(0) = 1 marks the onset of solution non-existence for the steady-state asymptotic solution. Beginning with g(0) values in the 0.5 - 0.6 range, no steady state could be reached in the numerical integrations.

and $f_m^n = I_m^n \Delta\eta$. Here a superscript (n) is a time index, a subscript (m) is a space index, $\Delta\tau$ is the time step, $\Delta\eta$ is the grid spacing, and $s \equiv \Delta\tau/\Delta\eta^2$. The total number of grid points, m_{max}, is chosen to be large enough that any further increase in its value yields negligible change to the solution throughout the computational domain. In most of our experiments we have set s = 0.5 and $\Delta\eta$ = 0.02. To these equations we append the boundary values arising from (2.31) - (2.34) (imposed for $\tau > 0$) and the initial conditions for no motion and no thermal perturbations. In (2.31) we take infinity to be any value large enough that any further increase in its value produces negligible change in the solution throughout the computational domain.

For the nondivergent flow variables, the FTCS discretization of (2.37) and (2.38) with Pr = 1 results in the update formulas

$$h_m^{n+1} = h_m^n + \Delta\tau\, k_m^n\left(1 - g_m^n\right) + \Delta\tau\,\Delta\eta\, I_m^n + 0.5\,\Delta\tau\, I_m^n\left(h_{m+1}^n - h_{m-1}^n\right) + s\left(h_{m+1}^n - 2h_m^n + h_{m-1}^n\right), \tag{5.4}$$

$$k_m^{n+1} = k_m^n\left(1 - \Delta\tau\, F_m^n\right) + \Delta\tau\left(G_\infty^n - G_m^n\right) + 0.5\,\Delta\tau\, I_m^n\left(k_{m+1}^n - k_{m-1}^n\right) - \Delta\tau\, h_m^n + s\left(k_{m+1}^n - 2k_m^n + k_{m-1}^n\right), \tag{5.5}$$

where

$$G_m^n = G_{m-1}^n + 0.5\,\Delta\eta\left(g_{m-1}^n + g_m^n\right); \quad m \geq 2,$$

$$= 0; \qquad m = 1\ . \quad (5.6)$$

The value G_∞^n in (5.5) corresponds to the value of G_m^n at the top of the computational domain, that is, at m = m_{max}.

The numerical integrations confirm the result from the asymptotic analysis that steady-state solutions do not exist if the along-slope buoyancy gradient g(0) exceeds a threshold value. However, in the numerical integrations, the threshold value for g(0) appeared to be in the range 0.5 - 0.6 rather than the value of 1.0. The positive value of this threshold indicates flow deceleration, that is, a weakening of katabatic flow in the downslope direction or strengthening of anabatic flow in the downslope direction.

As the threshold value in the numerical experiments was approached, the gravitational oscillations that developed in the solution grew to larger amplitude, and took longer to damp out. For values of g(0) that just exceeded the threshold value, a quasi-periodic regime was eventually established. However, for still larger values of g(0), the integration became unstable. It is not clear at this point whether the instability was purely computational or a consequence of an overly-constrained dynamical model. Clearly, the similarity model is inconsistent with a hydraulic jump, a structure known to occur in strongly decelerating katabatic flows (e.g., Renfrew 2004).

For all numerical experiments in which negative values of g(0) were prescribed (values were between -0.1 and -1000), a steady state was always obtained (as in the asymptotic solution). Steady state values of the remote slope-normal velocity component from the numerical integrations are compared with the analytical values obtained from (3.11) in Figs 3 and 4. A remarkable agreement is found between the asymptotic theory and the numerical integrations.

Other numerical experiments showed that the steady state structure was independent of the manner in which the surface forcing was imposed, that is, whether the surface forcing g(0) was imposed impulsively or was gradually ramped up to its full value after a specified period of time. Moreover, the threshold value of g(0) for breakdown of the steady state was found to be independent of the manner in which the surface forcing was imposed.

Results pertaining to the detailed structure of the flow variables in the steady state will be presented at the conference.

5. REFERENCES

Cushman-Roisin, B., 1984: An exact analytical solution for a time-dependent, elliptical warm-core ring with outcropping interface. *Ocean Modelling* **59**, 5-6.

Cushman-Roisin, B., W. H. Heil, and D. Nof, 1985: Oscillations and rotations of elliptical warm-core rings. *J. Geophys. Res.* **90**, 11756-11764.

Cushman-Roisin, B., 1987: Exact analytical solutions for elliptical vortices of the shallow-water equations. *Tellus* **39A**, 235-244.

Elder, J. W., 1965: Laminar free convection in a vertical slot, *J. Fluid Mech.*, **23**, 77-98.

Fletcher, C. A. J., 1988: Computational Techniques for Fluid Dynamics, Vol. 1. Springer-Verlag, 409 pp.

Gebhart, B., Y. Jaluria, R. L. Mahajan, and B. Sammakia, 1988: *Buoyancy-Induced Flows and Transport*. Hemisphere, 971 pp.

Gill, A. E., 1966: The boundary layer regime for convection in a rectangular cavity. *J. Fluid Mech.*, **26**, 515-536.

Gill, A. E., and A. Davey, 1969: Instabilities of a buoyancy-driven system. *J. Fluid Mech.*, **35**, 775-798.

Grisogono, B., and J. Oerlemans, 2001: Analytic solution for gradually varying eddy diffusivities. *J. Atmos. Sci.*, **58**, 3349-3354.

Grisogono, B., and J. Oerlemans, 2002: Justifying the WKB approximation in pure katabatic flows. *Tellus A*, **54**, 453-462.

Gutman, L. N., and V. M. Malbakhov, 1964: On the theory of katabatic winds of Antarctica. Meteor. Issled., 150-155.

Gutman, L. N., 1983: On the theory of the katabatic slope wind. *Tellus A*, **35**, 213-218.

Gutman, L. N., and J. W. Melgarejo, 1981: On the laws of geostrophic drag and heat transfer over a slightly inclined terrain. *J. Atmos. Sci.*, **38**, 1714-1724.

Lykosov, V. N. and L. N. Gutman, 1972: Turbulent boundary layer above a sloping underlying surface. *Izv. Acad. Sci. USSR, Atmos. Ocean. Phys.*, **8**, 799-809.

Madsen, O. S., 1977: A realistic model of the wind-induced Ekman boundary layer. *J. Physical Ocean.*, **7**, 248-255.

Oerlemans, J., 1998: The atmospheric boundary layer over melting glaciers. *Clear and Cloudy Boundary Layers* (A. A. M. Holtslag and P. G. Duynkerke, Eds.), Royal Netherlands Academy of Arts and Sciences, 129-153.

Pedlosky, J., 1987: *Geophysical Fluid Dynamics*, Springer-Verlag, New York, 710 pp.

Phillips, O. M., 1970: On flows induced by diffusion in a stably stratified fluid. *Deep-Sea Res.*, **17**, 435-443.

Prandtl, L., 1942: *Führer durch die Strömungslehre*, Vieweg und Sohn, Braunschweig, 382 pp.

Renfrew, I. A., 2004: The dynamics of idealized katabatic flow over a moderate slope and ice shelf. *Q. J. Roy. Meteor. Soc.*, **130**, 1023-1045.

Schlichting, H., 1979: *Boundary-Layer Theory*, McGraw-Hill, New York, 817 pp.

Shapiro, A., 1996: Nonlinear shallow-water oscillations in a parabolic channel: exact solutions and trajectory analyses. *J. Fluid Mech.*, **318**, 49-76.

Shapiro, A., 2001: A centrifugal wave solution of the Euler and Navier-Stokes equations. *J. Appl. Math. Phys. (ZAMP)*, **52**, 913-923.

Shapiro, A., and E. Fedorovich, 2004: Prandtl number dependence of unsteady natural convection along a vertical plate in a stably stratified fluid. *Intl. J. Heat Mass Transfer*, **47**, 4911-4927.

Thacker, W. C., 1981: Some exact solutions to the nonlinear shallow-water wave equations. *J. Fluid Mech.* **107**, 499-508.

Veronis, G., 1970: The analogy between rotating and stratified fluids. *Annu. Rev. Fluid Mech.*, **2**, 37-66.

Wunsch, C., 1970: On oceanic boundary mixing. *Deep-Sea Res.*, **17**, 293-301.

Williams, J. C., 1968: Nonsteady stagnation-point flow, *AIAA Journal* **6**, 2417-2419.

Zandbergen, P. J. and D. Dijkstra, 1987: Von Kármán swirling flows. *Annu. Rev. Fluid Mech.* **19**, 465-491.